Time-Resolved MR Angiography With Limited Projections

Yuexi Huang[1,2*] and Graham A. Wright[1,2]

A method for reconstruction of time-resolved MRI called highly-constrained backprojection (HYPR) has been developed. To evaluate the HYPR reconstruction in relation to data sparsity and temporal dynamics, computer simulations were performed, investigating signal modulations under different situations that reflect dynamic contrast-enhanced MR angiography (MRA). In vivo studies were also performed with gadolinium diethylene-triamine pentaacetic acid (Gd-DTPA) for abdominal MRA in a canine model to demonstrate the application of HYPR for three-dimensional (3D) time-resolved MRA. When contrast dynamics vary over space, large vessels (e.g., veins) tend to introduce signal interference to small vessels (e.g., arteries) in HYPR, particularly when the vessels are in close proximity. The enhancement of background tissue signals may also alter the arterial and venous temporal profiles in HYPR. However, the artifacts are manifest as intensity modulation rather than structural interference, and therefore have little impact on structural diagnosis. Increasing the number of projections per time point increases temporal blur while reducing corruption of temporal behavior from adjacent tissues. Uniformly interleaved acquisition order, such as the bit-reversed order, is important to reduce artifacts. With high signal-to-noise ratio (SNR) and limited artifacts, HYPR reconstruction has potential to greatly improve time-resolved MRA in clinical practice. Magn Reson Med 58: 316–325, 2007. © 2007 Wiley-Liss, Inc.

Key words: HYPR; MR angiography; limited projections; AUCTION; time-resolved

Spatial resolution, temporal resolution, signal-to-noise ratio (SNR), field of view (FOV), and the extent of artifacts are common tradeoffs in magnetic resonance imaging (MRI). This is particularly an issue in contrast-enhanced studies such as peripheral MR angiography (MRA), in which contrast dynamics are often of interest for revealing pathological information and for timing the acquisition to the peak arterial enhancement. Submillimeter spatial resolution is necessary to visualize small arteries, large three-dimensional (3D) imaging volumes are needed to provide coverage of the lower extremities, sufficient SNR is mandatory, and artifacts cannot interfere with clinical evaluations. In current clinical practice, a tradeoff is made sacrificing temporal resolution in order to gain sufficient spatial resolution. That is, static 3D volumes are acquired, in which the arterial signals are a weighted average of the contrast enhancement throughout the data acquisition. Although elliptical-centric ordered acquisition (1,2) and the application of parallel imaging techniques (3) have greatly improved the robustness of the current protocols, mistiming of the contrast enhancement and venous contamination are still potential issues due to the often irregular blood-flow patterns in the patient population (4).

Alternatively, contrast-enhanced MRA can be performed in a time-resolved manner by taking advantage of the data sparsity to shorten the data acquisition and to optimize reconstruction. Projection reconstruction (PR) techniques achieve high undersampling factors with acceptable artifacts due to the limited artifactual interference caused by high-frequency undersampling of sparse data sets (5,6). The acceptable undersampling factors in PR are approximately six in two dimensions and 50 in three dimensions. Recent work with limited view projections (7) and highly constrained backprojection (HYPR) (8) incorporated a composite image as the prior knowledge of the object, thus further leveraging the undersampling factor. When combined with time-resolved imaging of contrast kinetics (TRICKS) (9), HYPR achieved a 3D undersampling factor of 225. More significantly, the SNRs of limited-projection data sets reconstructed by HYPR are at comparable levels to those of the composite data set. This is seemingly counterintuitive since SNR should decrease with the reduction of acquisition time. A better understanding of the advantages and potential limitations of the HYPR algorithm is needed as part of the development of this new technique. In this paper, the original HYPR algorithm is slightly modified so that it linearly converges to the composite image as the number of the limited projections increases. The SNR behavior and potential artifacts of HYPR are demonstrated by computer simulations. Contrast-enhanced studies were performed to evaluate the effectiveness of HYPR with in vivo data.

MATERIALS AND METHODS

In the original HYPR algorithm, the formula for the reconstruction is

$$\mathrm{HYPRimage}(x,y,z) = (1/N_{pr}) * C(x,y,z) * \Sigma[P(r,\theta,\phi)/P_c(r,\theta,\phi)] \quad [1]$$

where N_{pr} is the number of limited projections in the time frame, $C(x,y,z)$ is the time-averaged composite image, $P(r,\theta,\phi)$ is the unfiltered backprojection of a certain raw projection, and $P_c(r,\theta,\phi)$ is the unfiltered backprojection of the corresponding projection calculated from the composite image.

Since the profiles of the projection lines are normalized (divided) before they are summed, this is a nonlinear process. As the number of the limited projections increases toward the total number of projections, the HYPR image

[1]Department of Medical Biophysics, University of Toronto, Toronto, Canada.
[2]Sunnybrook Health Sciences Centre, Toronto, Canada.

Grant sponsors: Canadian Institutes of Health Research; GE Healthcare.

*Correspondence to: Yuexi Huang, Imaging Research, Sunnybrook Health Sciences Centre, C736D-2075 Bayview Avenue, Toronto, Ontario, M4N 3M5, Canada. E-mail: huangyx@sten.sunnybrook.utoronto.ca

Received 24 August 2006; revised 12 April 2007; accepted 26 April 2007.
DOI 10.1002/mrm.21312
Published online in Wiley InterScience (www.interscience.wiley.com).

should be equal to the composite image. However, this is not necessarily true in the original equation. Therefore, we modified the original equation to

$$\text{HYPRimage}(x,y,z) = C(x,y,z) * [\Sigma P(r,\theta,\phi)/\Sigma P_c(r,\theta,\phi)] \quad [2]$$

in which the limited projections are backprojected and summed to form an image before it is normalized by the corresponding limited-projection image calculated from the composite image. As the number of the limited projections increases to be equal to the total number of projections of the composite image, $[\Sigma P(r,\theta,\phi)/\Sigma P_c(r,\theta,\phi)] = 1$, and the HYPR image is equivalent to the composite image $C(x,y,z)$.

If the image of limited projections $\Sigma P(r,\theta,\phi)$ is reconstructed by filtered-backprojection using the standard filter designed for full projection acquisition, its SNR will be substantially lower than that of the composite image $C(x,y,z)$. The SNR of the HYPR image therefore will be dominated by the low SNR of the limited projection image. HYPR reconstruction solves this issue by using unfiltered backprojection to reconstruct the limited-projection image. Unfiltered backprojection has a significantly higher SNR than filtered backprojection due to the over-weighting of the low frequency data (data at the center of the *k*-space). The cost of unfiltered backprojection is the unequal weighting and blurring of the object profiles. This is not an issue if signal intensities change proportionally in the projection dimension, so that the projection profile after normalization is flat. However, if this assumption is not valid, the error/artifacts introduced depend on the image sparsity and size of the objects. For the applications of contrast-enhanced MRA, since the cross-sections of vessels are small and images are sparse, the artifacts associated with the unfiltered backprojection should be limited.

Simulations

A 2D computer model was created to demonstrate the basic properties of the modified HYPR algorithm. The signal intensity of a circular shaped object with 50 pixels in diameter increased linearly during the acquisition of the 2D PR data. A total of 128 projection lines were acquired while the signal intensity of the object increased from one to 128 units (Fig. 1a). The 128 projections were acquired at various angles in a bit-reversed order to more evenly cover

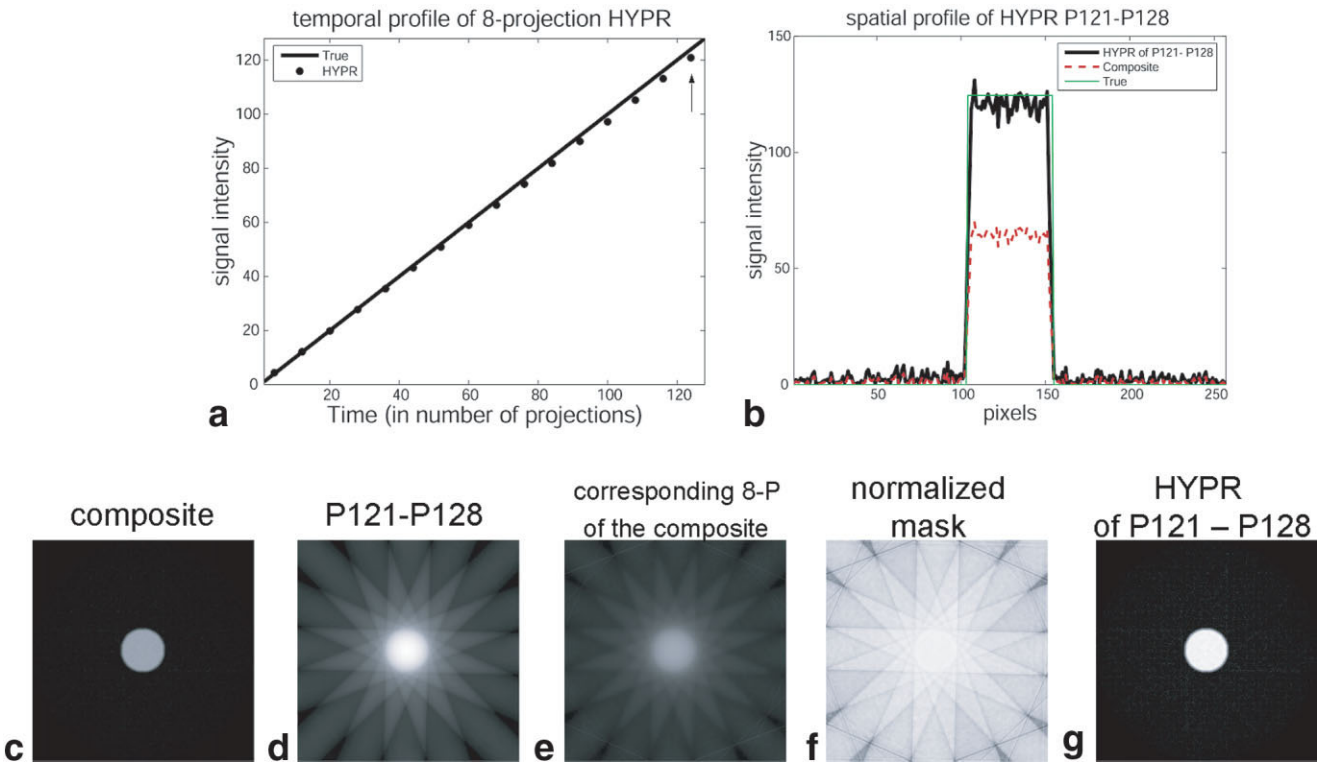

FIG. 1. Simulation of HYPR reconstruction of a circular dynamic model. The temporal profile of signal intensity changes is shown in image (**a**). The stars indicate the HYPR reconstructed temporal profile for every eight projections, while the solid line is the true profile as a reference. The spatial profile of the last HYPR temporal frame (the last eight projections, indicated by an arrow in image a) is shown in image (**b**). Image (**c**–**g**) illustrate the HYPR reconstruction process of the modified algorithm for the temporal frame by the last eight projections. Image (c) is the composite image reconstructed by the filtered backprojection algorithm using all 128 projections. Image (d) is the unfiltered backprojection of the last eight projections. Image (e) is the corresponding eight projections calculated from the composite image (c). Note that they present similar streak artifacts but at different intensities. Image (f) is the normalized mask image formed by dividing image (d) and (e). The average intensity of the mask in the region of the object is approximately two. Image g is the HYPR reconstructed image obtained by multiplying the normalized mask (f) with the composite image (c). The average intensity of the object in image (g) is amplified to twice that of the composite image. Note the noise is also amplified by a factor of two, leaving the SNR of the HYPR image close to that of the composite image. [Color figure can be viewed in the online issue, which is available at www.interscience.wiley.com.]

the *k*-space over time (10). A total of eight projections were grouped together for each HYPR reconstruction of the temporal images. In total 16 temporal images were reconstructed. The eight-projection image, which was reconstructed by unfiltered backprojection, was normalized by the corresponding eight-projection image calculated from the composite image before being multiplied by the composite image. Both the temporal profiles and spatial profiles of the HYPR reconstruction were compared to the true profiles.

HYPR reconstruction was developed under the assumptions of data sparsity and uniformity of signal dynamics. When data is less sparse, or signals of different objects in the FOV change nonuniformly, HYPR is expected to modulate image contrast and induce artifacts if an insufficient number of projections are used. The magnitude of the modulation was investigated by a four-object computer model, in which two objects represent arteries and two objects represent veins. The diameter of each arterial object is approximately 10 pixels, and the venous diameters are approximately 18 pixels. The arterial signals increased earlier than the venous signals to simulate the contrast enhancement in MRA studies. Eight projections were grouped together for HYPR reconstruction. To increase the temporal resolution, sliding window reconstruction was applied to update one of the eight projections at each time step. The distance between the objects was varied from 64 pixels to 16 pixels to test the effect of data sparsity on signal interference in HYPR. The number of projections in each HYPR group was varied from one to 32 to investigate the tradeoff of temporal and spatial blurring. The temporal profiles and spatial profiles of the HYPR reconstruction were compared to the true profiles to illustrate the magnitude of the modulation by contrast dynamics.

To evaluate the impact of HYPR reconstruction on the detection of stenoses, one of the arterial objects in the four-object model was modified to form a crescent shape to simulate the structural situation of a stenosis. The same temporal profiles of the arterial and venous enhancement as in the previous simulations were used. The possibility of turbulent flows at the site of stenosis was not included in the current model due to the difficulty of simulating the complicated patterns in turbulent flows. However, if the *k*-space is sampled relatively uniformly, as is the case in our model by the bit-reversed ordering of the projection angles, the turbulent flow is not expected to introduce significant structural artifacts. This needs to be validated by future in vivo studies.

In contrast-enhanced MRA with an extravascular agent, not only signals in major arteries and veins are increased; capillary and tissue signals are also enhanced due to the perfusion and subsequent leakage of the contrast agent into the tissue bed. Although the increase of capillary and background tissue signals is not as significant as that in major vessels on a per volume basis, the signal increase in the projection images could be significant due to the large volume of background tissues along the projection dimension. The increase of background signals reduces data sparsity and is expected to introduce artifacts to vascular signals in HYPR reconstruction. A simulation was performed to evaluate the effect of background enhancement on HYPR reconstruction. A circular background region (64 pixels in diameter) was added to the four-object model discussed earlier. Signals in the background region increase linearly over the first-pass of the contrast agent from zero to a quarter of the steady state vascular intensity. HYPR reconstruction using the same characteristics as in the previous models was performed to compare the vascular signals with and without background enhancement.

In Vivo Experiments

Contrast-enhanced studies were performed on two canines to apply the HYPR reconstruction to in vivo data sets. The study protocol was approved by our institutional Animal Care Committee. 14 ml of contrast agent (Omniscan, Nycomed) was injected manually followed by 20 ml of saline flush (contrast dose 0.2 mmol/kg). A total of 64 2D projections at different angles were acquired during the injection to fill the full 3D *k*-space. The rotation of the projection angle was achieved by rotating the logical axes of a 2D fast spoiled gradient echo (SPGR) sequence (GE 1.5T Excite). The SPGR sequence was modified for this purpose with the following characteristics: four-channel surface coil for signal reception, FOV = 25 × 25 cm, matrix size = 256 × 256, slice thickness = 250 mm, TR = 3.9 ms, flip angle = 20°, bandwidth (BW) = 125 kHz, and temporal resolution ≈ 1 s/projection. A mask data set was acquired before the contrast injection for complex subtraction. The angles of the 64 projections were chosen in the bit-reversed order as in the simulations. Eight projections were grouped for HYPR reconstruction, which gave a true temporal resolution of 8 s per 3D data set. Sliding-window reconstruction was applied to smooth the temporal resolution to 2 s by updating two of the eight projections for each time point.

The effect of background enhancement on HYPR reconstruction was evaluated by measuring the temporal signal intensities of regions-of-interest (ROIs) on the descending aorta, vena cava and adjacent background tissues in the HYPR images. The significance of the increase in background signals in the projection images was also verified by a subsequent in vivo study in a separate animal study. This study was performed by repeatedly acquiring a single-view, 2D slab projection coronal image so that the temporal profiles in the projection images can be measured. The ROIs of the arterial and venous signals in the projection images were from similar regions of the aorta and vena cava as in the HYPR images, and the ROI of the background tissue was taken close to the aorta.

RESULTS

Simulation results of the circular dynamic model are shown in Fig. 1. The temporal profile of the HYPR reconstruction is close to the true profile in Fig. 1a. The spatial profile of the last HYPR temporal frame, which corresponds to the last eight projections, is shown in Fig. 1b. The signal intensity of the object in this frame is 125 units (the average of 121 to 128 units), compared to a signal intensity of 64 units in the composite image. Fig. 1c–g illustrate the HYPR reconstruction process for this temporal frame using the modified algorithm (details in the caption). The streaks in the normalized mask are also transferred to the HYPR image but at low intensities due to the

lack of signals at the corresponding pixels in the composite image.

The simulation results of the nonuniform dynamic model are shown in Fig. 2 and 3. The object sizes and dynamics are the same in the two figures. The only difference is that the distance between the arterial and venous objects in Fig. 2 is four times larger than the distance used in Fig. 3 (64 pixels vs. 16 pixels). In Fig. 2a, the temporal profiles of the arterial and venous signals with HYPR reconstruction in general follow the true profiles, except for obvious modulations near the peak arterial and venous enhancements. The spatial profile of the HYPR frame indicated by the arrow is shown in Fig. 2b. The arterial and venous signals are close to their true intensities (118 units and zero units, respectively), although there is slight venous amplification. Fig. 2c–g demonstrate the HYPR reconstruction of this time frame. Although in the raw limited-projection image (Fig. 2d) only the arterial signals have real values, the streaks of the arterial signals overlap the regions of the venous objects. Therefore, the venous signals cannot be totally normalized to the zero level in the HYPR image.

In Fig. 3, because the objects are closer together, the cross-talk of their streaks is more significant than in Fig. 2. In the temporal profiles in Fig. 3a, there are more signal modulations in the arterial and venous profiles. Particularly, there is more venous enhancement before the peak arterial enhancement, and the arterial signals at the peak venous enhancement are even higher than at the peak arterial enhancement. This is also reflected in the spatial profile in Fig. 3b. This is the same time frame as that in Fig. 2b, but the arterial and venous signals both deviate significantly from the true intensities. However, despite the increased modulation of signal intensities, the relative artery-vein contrast is substantially preserved in the HYPR reconstruction.

The effect of cross-talk between objects can be reduced by increasing the number of limited projections in each HYPR image. Figure 4 shows the reconstruction of a similar model as in Fig. 3, except the sizes of the four objects are the same. When 32 projections are used for each HYPR image, as shown in Fig. 4a, the temporal signals are blurred by averaging more projections for each HYPR frame. However, the interference between objects is reduced resulting in smoother temporal profiles. As the number of projections in each HYPR frame decreases (Fig. 4b–f), the true temporal resolution increases, but the cross-talk between objects causes more fluctuations in the profiles.

HYPR reconstruction of the stenosis model is shown in Fig. 5. The same time frame as that in Fig. 3 is shown. Comparing the composite image (Fig. 5a) with the HYPR image (Fig. 5e), there is no obvious structural artifact at the site of the arterial stenosis in either case. The venous signals are not normalized to zero at this time frame due to the cross-talk from the arterial signals, as in Fig. 3. The

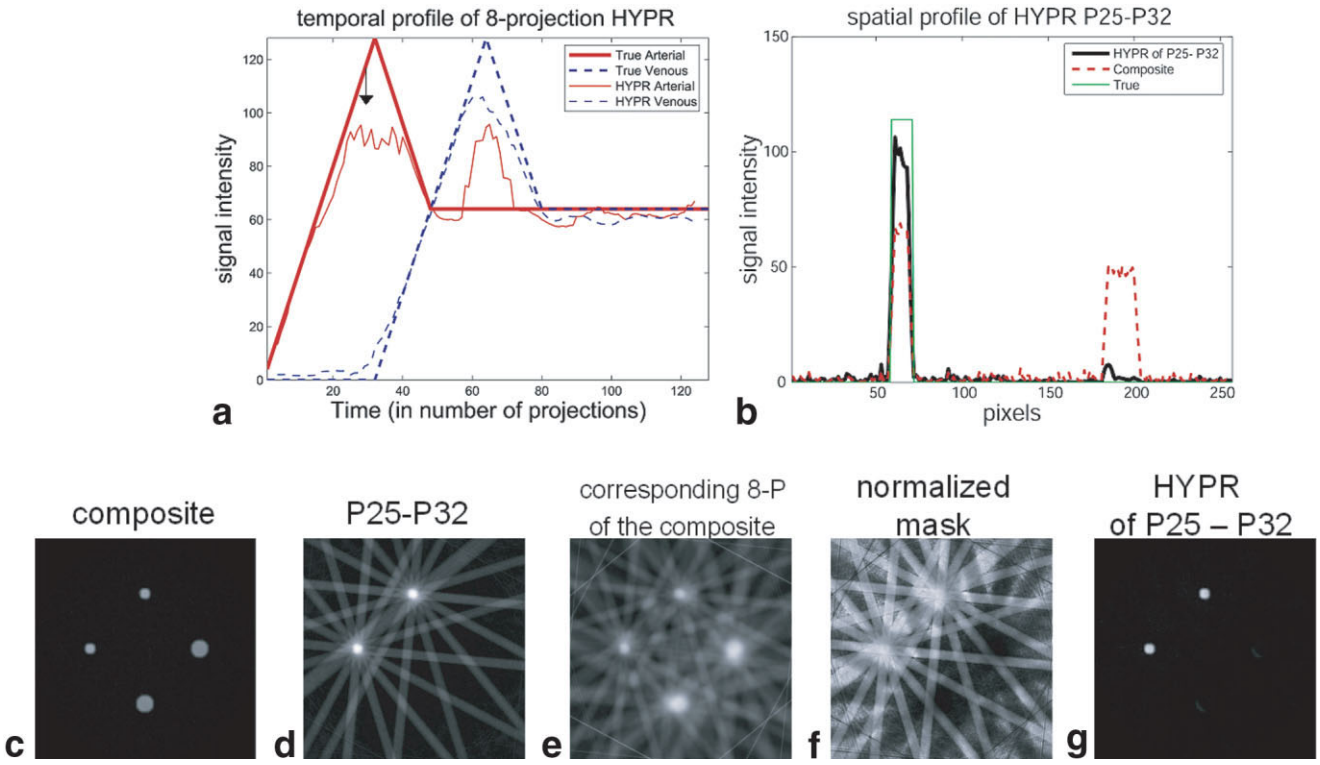

FIG 2. Simulation of HYPR reconstruction of a sparse-object model with nonuniform dynamic changes. The two smaller objects simulate the arterial signals in contrast-enhanced studies, while the two larger objects simulate the venous signals. The arterial enhancement is earlier than the venous enhancement, as illustrated in image (**a**). The spatial profile of the HYPR frame indicated by the arrow in image a is shown in (**b**). Image (**c**–**g**) illustrate the HYPR reconstruction of this time frame as the same order as in FIG. 1. [Color figure can be viewed in the online issue, which is available at www.interscience.wiley.com.]

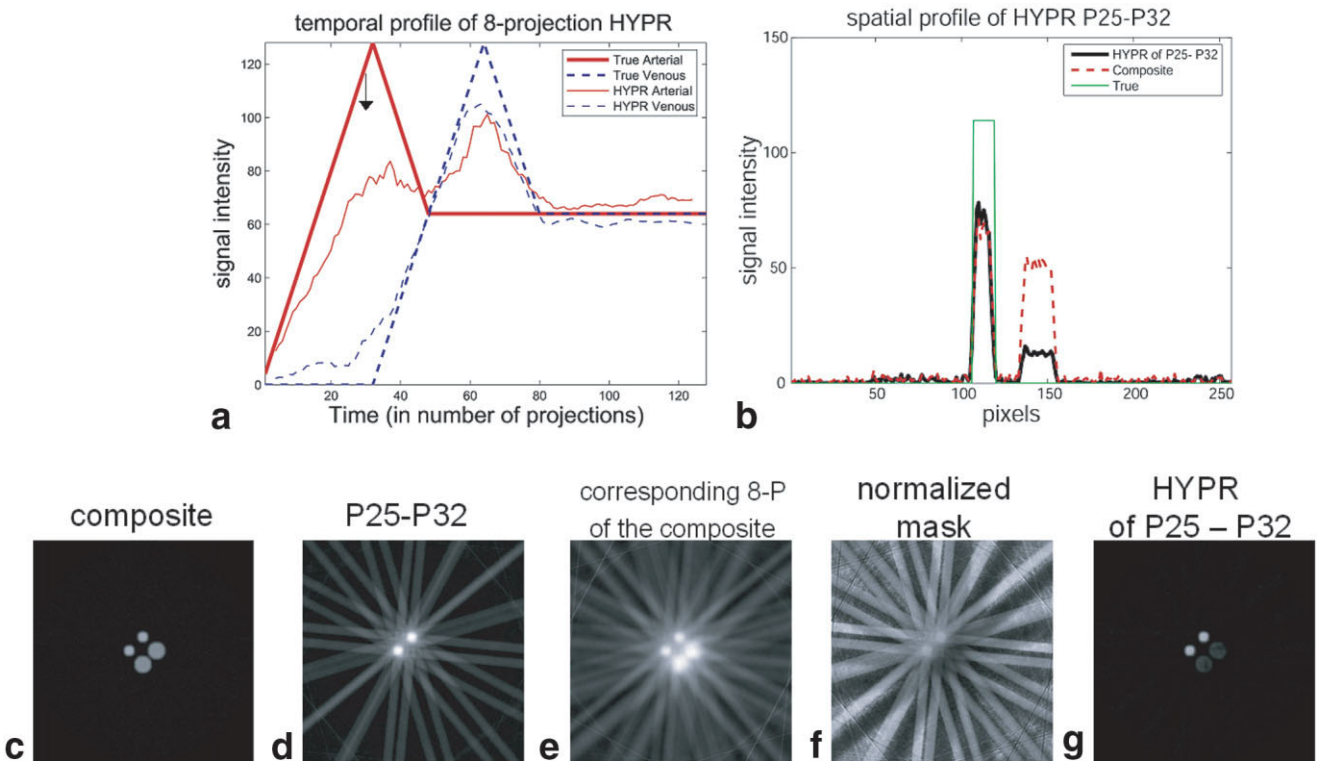

FIG 3. Simulation of HYPR reconstruction of a less-sparse model than that in FIG. 2. The only difference from the model in Fig. 2 is that in this figure the objects are closer to each other. The HYPR reconstruction causes more significant modulation of the temporal profiles, especially to the first-pass arterial signals. [Color figure can be viewed in the online issue, which is available at www.interscience.wiley.com.]

dark bands that appear in the venous regions in Fig. 5 also appear in Fig. 3; therefore, they are not specifically due to the shape of the stenosis. The dark bands are caused by the normalization of the arterial streaks in the venous regions in Fig. 5b to the venous signals in the limited-projection composite image (Fig. 5c). In later time frames, because the venous signals also appear in the limited projection image, the dark bands are less significant.

The simulation of the effect of background enhancement on HYPR reconstruction is shown in Fig. 6. The enhancement of background signals significantly modulated the arterial and venous signals as shown in Fig. 6a, comparing to the case without background enhancement in Fig. 3a. Particularly, the HYPR arterial signal in Fig. 6a stays at its peak enhancement level after the first-pass, rather than dropping to the steady state level as in Fig. 3a. This also can be seen in the reconstruction of a steady state HYPR frame in Fig. 6c–g. The background signals reduce the artery-vein contrast in Fig. 6d and e; therefore the normalized mask Fig. 6f fails to modulate the arterial signals to the true steady-state level after multiplication with the composite image Fig. 6c. In Fig. 6g, the arterial signals are still higher than the venous signals as in the composite image. In contrast, because background signals are still at relatively low intensities in the first pass, the artery-vein contrast in the peak-arterial HYPR frame (Fig. 6b) is similar to that without background enhancement (Fig. 3g).

The result of an in vivo study is shown in Fig. 7. The top two rows are maximum intensity projection (MIP) images from the front-view (0 degrees), and the bottom two rows are views from 135 degrees. The first-pass arterial and venous enhancements are clearly visualized in 3D every two s. The SNRs of the temporal data sets after the peak arterial enhancement are similar to the composite data set.

The ROIs on the aorta, vena cava and background tissues in a cross-sectional HYPR image are shown in Fig. 8a. Their temporal profiles are shown in Fig. 8b. As expected by the simulation in Fig. 6, the arterial and venous signals after the first pass did not drop to a similar level in the steady state. The increase of background signals in projection images is verified by the time-resolved 2D projection study. As shown in Fig. 8c, the increase in background tissue signals is significant in the projection images. The measured arterial and venous signals in the projection images are an average of the vessels signals with the background tissue signals along the projection dimension. Therefore, there is no significant drop of the arterial and venous signals after the first pass. However, if we assume the sizes of vessels are relatively small compared to the background tissues in the projection dimension, the arterial and venous signals can be adjusted by subtracting the adjacent tissue signals. As shown in Fig. 8d, after this adjustment, the arterial and venous signals drop to a similar steady-state level as expected. This confirms that the increase in background signals in the projection images artificially modulates vascular signals in HYPR reconstruction.

DISCUSSION

Spatial and temporal resolution are normally traded off in image acquisition. However, with HYPR reconstruc-

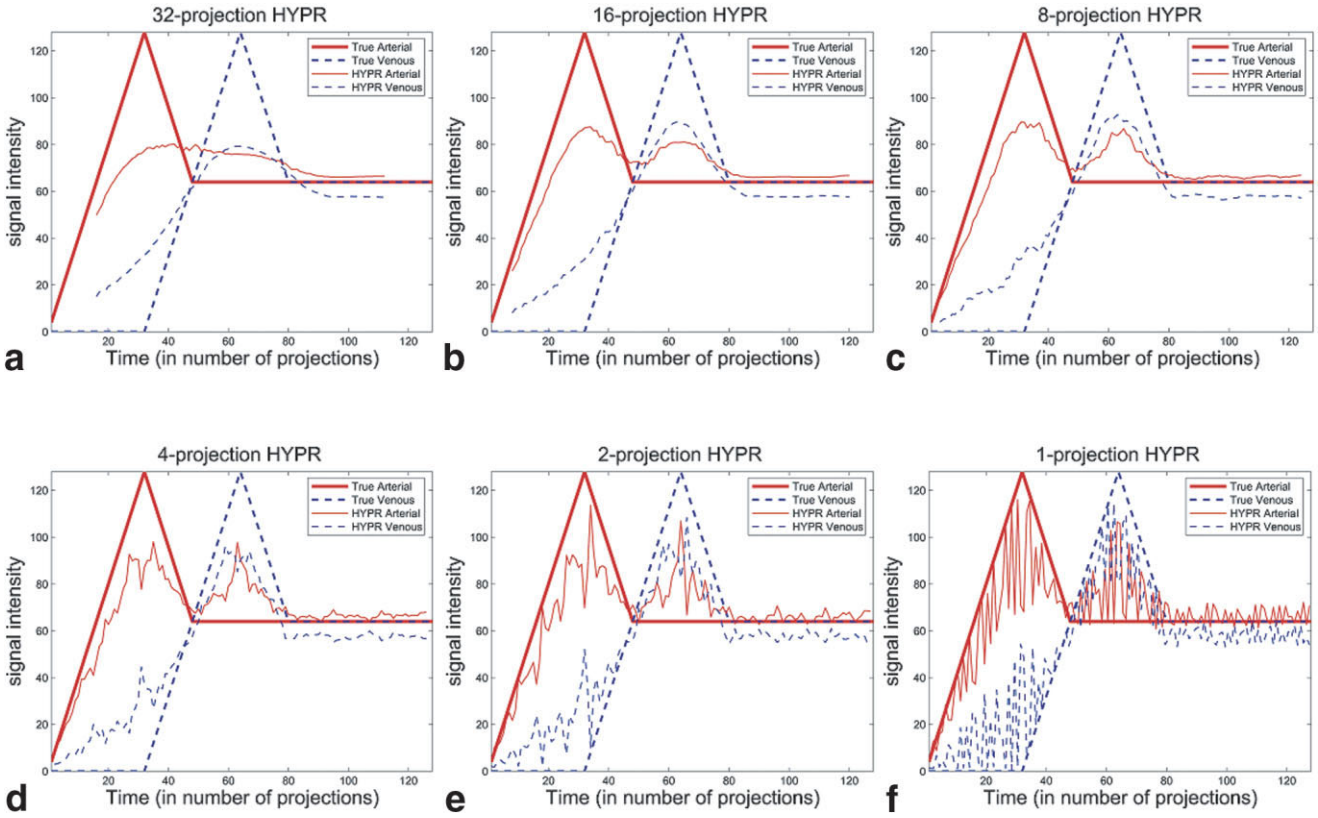

FIG 4. The modulation of temporal profiles by the number of limited projections in HYPR. Sliding window reconstruction was applied for updating one projection for each HYPR reconstruction. As the number of the limited projections decrease, the temporal profile has a higher true resolution. However, the interference between the objects causes fluctuation in signal intensities. [Color figure can be viewed in the online issue, which is available at www.interscience.wiley.com.]

tion, the control of the spatial resolution and temporal resolution are separated into contributions from the composite image and the normalized limited-projection image, respectively. The composite image has full spatial resolution but low temporal resolution, while the limited-view projection image has high temporal resolution but lower spatial resolution and more streak artifacts. The multiplication of the two images combines the advantages and disadvantages of both images. However, under the assumption of uniform dynamic changes across the FOV, the artifacts are proportional between the limited-projection image and the corresponding limited-projection image calculated from the composite, and cancel each other out after normalization. Therefore, under the assumption of uniform dynamics, HYPR reconstruction achieves both high spatial and high temporal resolution.

Under the nonuniform dynamics as always occurs in practice, the combination introduces artifacts to the HYPR image. However, for sparse data sets, the interference of the nonuniform dynamics is relatively minor in terms of the overall image contrast. This is demonstrated by computer simulations in this study. It is important to note that data sparsity is not only related to the number of structural pixels in the FOV, but also the distance between the structures (or the density of the structure region). This is demonstrated in Figs. 2 and 3. With the only difference being signal density, more artifacts are induced in Fig. 3 due to

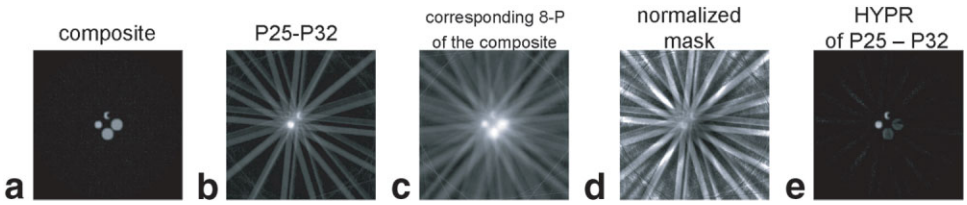

FIG 5. Simulation of HYPR reconstruction of a stenosis model. One of the arterial objects in the model used in Fig. 3 was modified to form a crescent shape to simulate the structural situation of a stenosis. All other characteristics are the same as FIG. 3. There is no obvious structural artifact at the site of the stenosis in either the composite or HYPR images. [Color figure can be viewed in the online issue, which is available at www.interscience.wiley.com.]

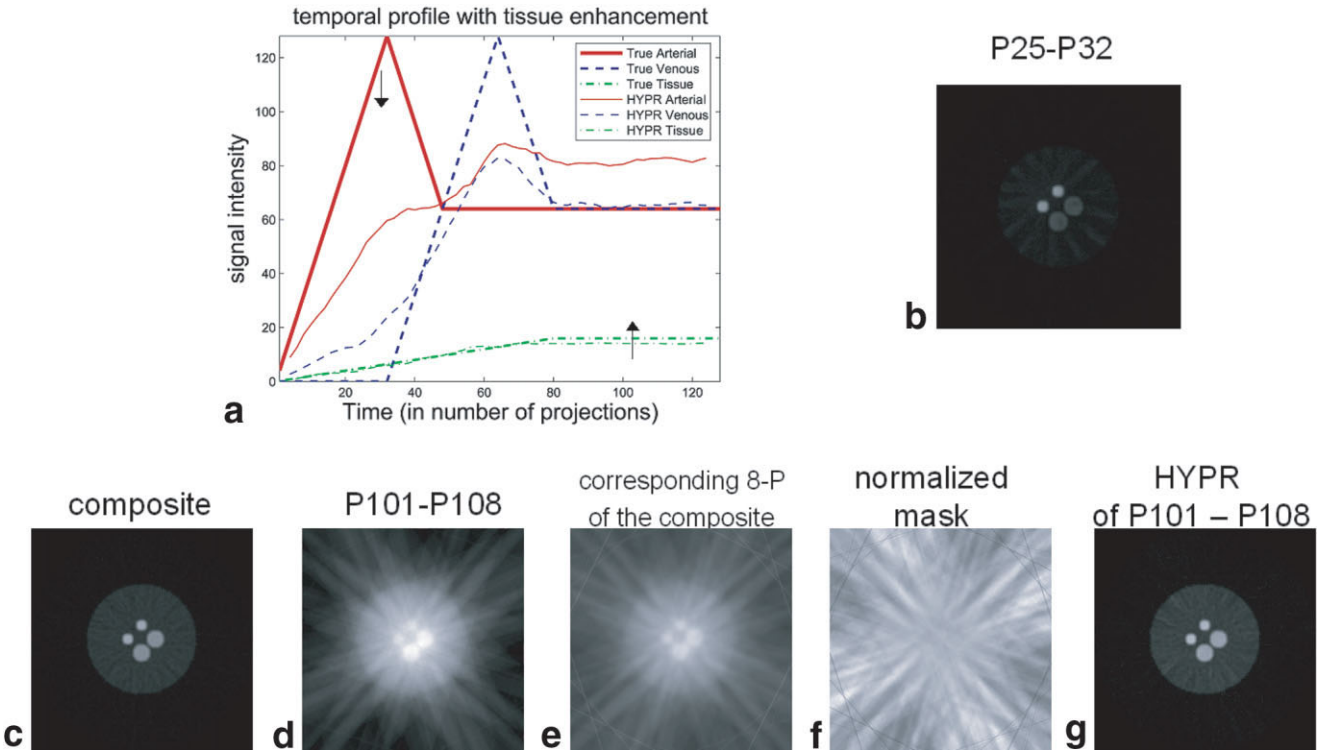

FIG 6. Simulation of the impact of background enhancement on HYPR reconstruction. The increase in background signals modulates both the arterial and venous temporal profiles as shown in (**a**), when compared to the case without background enhancement in Fig. 3a. (**b:** shows the peak-arterial HYPR frame P25-32 (corresponding to the down arrow in [a]), in which the artery-vein contrast remains to be similar to the situation without background enhancement (Fig. 3g). However, as shown by (**c–g**), HYPR reconstruction significantly increases the arterial level at the steady state (corresponding to the up arrow in [a]). In (g), arterial signals are still higher than venous signals in the steady-state HYPR frame. [Color figure can be viewed in the online issue, which is available at www.interscience.wiley.com.]

greater interference among the objects. We also found the absolute positions of the objects have no impact on artifacts in HYPR reconstruction. For example, if the four objects in Fig. 3 are moved to a corner away from the center of the FOV, the characteristics of the artifacts still hold.

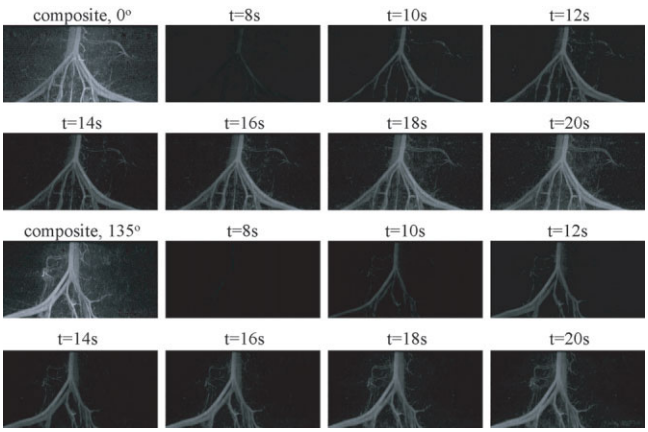

FIG 7. HYPR reconstruction of in vivo data. The true temporal resolution is 8 s/3D data set, which is interpolated to 2 s by sliding window reconstruction. The composite and HYPR temporal images from the 0° and 135° views are shown. The arterial enhancement and the venous enhancement can be separated in the HYPR frames. The SNR of the temporal frames is comparable to that of the composite image. [Color figure can be viewed in the online issue, which is available at www.interscience.wiley.com.]

In contrast-enhanced MRA studies, since the veins are often in close proximity to the corresponding arterial segments, the cross-talk of their signals should be at a level similar to that in Fig. 3. This is verified in the in vivo study as shown in Figs. 7 and 8. As expected, the venous signals increase before the peak arterial enhancement in the HYPR images due to the cross-talk from the arterial enhancement. Nevertheless, the arterial signals are significantly higher than the venous signals; therefore arteries still appear to be enhanced earlier than the veins in Fig. 7. However, the increase in background tissue signals in the projection images significantly amplified the arterial and venous signals. Particularly, the artery-vein contrast in the steady state is modulated. Although the use of intravascular contrast agents may help to suppress the tissue signals, the enhancement of the capillary-level small vessels in the background would still need to be considered. In peripheral MRA, the purpose of temporally resolved data sets is mainly to separate the arterial and venous enhancement and to avoid the difficulties associated with contrast timing. The route by which blood fills the vessels (e.g., antegrade vs. retrograde) may also be of clinical interest. However, the absolute and relative signal intensities of the arteries and veins may not be very important. Therefore, we do not expect the cross-talk to cause significant problems in peripheral MRA. On the other hand, the relative

signal intensity variation may be of particular interest in some applications such as perfusion imaging; therefore, one needs to be aware of HYPR-induced artifacts.

As suggested above, large objects cause more significant changes in signal intensities in the projections than small objects, even if their absolute intensities are the same. Therefore, in HYPR reconstruction, the signal changes of large objects will induce more signal interference in small objects. This also can be seen by comparing Figs. 3a and 4c. In Fig. 3a, the larger venous object causes more signal modulation to the arterial signals, compared to results in Fig. 4c, where the sizes of arterial and venous objects are the same.

As discussed in the methods section, unfiltered backprojection is applied instead of filtered backprojection to improve SNR of the limited-projection images. The appendix of the original HYPR work (8) provided a detailed analysis of the SNR behavior of HYPR images for the original algorithm. With the modified algorithm in this paper (Eq. [2]), the HYPR image is calculated from three images: the composite image $C(x,y,z)$, the unfiltered limited-projection image $P(r,\theta,\phi)$, and the corresponding unfiltered limited-projection image calculated from the composite $P_c(r,\theta,\phi)$. The SNR of the HYPR image therefore will be dominated by the image with the lowest SNR. If we assume the SNR of a circular shaped object in the composite image is SNR_c, the diameter of the object is N_v pixels, and the matrix size of the composite image is N_{pix} pixels, then the SNR of the object in a projection is approximately $SNR_c \cdot N_v/\sqrt{N_{pix}}$. If N_p projections are included for each HYPR group, then the SNR of $P(r,\theta,\phi)$ is approximately $SNR_c \cdot N_v/\sqrt{N_{pix}} \cdot \sqrt{N_p}$. The SNR of $P(r,\theta,\phi)$ will be approximately the same, depending on the dynamic change of the signal intensities of the object. Therefore, the SNR of the HYPR image depends on N_v, N_{pix}, and N_p. For example, for $N_v = 5$ pixels, $N_p = 16$ projections per HYPR group, $N_{pix} = 256$ pixels, the SNR of $P(r,\theta,\phi)$ and $P_c(r,\theta,\phi)$ is 1.25 times that of SNR_c. Therefore, the SNR of the HYPR image will be dominated by the composite image, which has the lowest SNR of the three. For smaller objects, the SNR of the HYPR image will be lower than that of the composite image, unless the number of limited projections is increased accordingly. It is important to note the reason that unfiltered backprojection has higher SNR than filtered backprojection is signal averaging with surrounding pixels (convolution with the Fourier transform of the gridding density function in *k*-space). If signals of every pixel in the FOV change proportionally, as in the underlying assumption of HYPR reconstruction, the artifacts due to the signal averaging will be cancelled after normalizing $P(r,\theta,\phi)$ and $P_c(r,\theta,\phi)$. However, if the dynamic changes vary spatially, the signal averaging in unfiltered backprojection will cause signal modulation. HYPR depends on data sparsity (the amount of zero-mean pixels) to minimize the artifacts. In the MRA application, we assume the signal modulation is not significant due to the nature of the sparse data sets.

Since the composite image is an average of all projections, it is important to arrange the projection acquisitions in a spatially uniform manner to avoid signal modulation due to the dynamic changes. If sequential angle order (or continuously rotating order) is applied, there will be significant artifacts in the composite image. Since these artifacts are not in the limited projections, they cannot be cancelled by normalization, and therefore will be transferred to the HYPR images. The uniform coverage of *k*-space is achieved by the bit-reversed order in this study (10). Bit-reversed order maximizes the angular difference between consecutive projections. It provides the flexibility of varying the number of limited projections used for each HYPR group in postprocessing. The limitation of bit-reversed order is that the number of acquisitions has to be a power of two. Alternatively, lattice-permutated order (11) or golden ratio–based ordering (12) can be investigated for more flexible control of the aliasing patterns.

The normalization process involves dividing signals of corresponding projections. If there are near-zero values in the denominator, the normalization will induce spike artifacts in the HYPR image. Therefore in the original published algorithm, a threshold is needed to avoid the near-zero pixels (Dr. Charles Mistretta, personal communication). In the modified algorithm, the denominator is the average of a number of projections and reduces the likelihood of near-zero values; therefore, no threshold is needed. On the other hand, the modified algorithm requires two unfiltered backprojections, compared to only one in the original algorithm. This lengthens the reconstruction time. Beyond these technical details, the two algorithms behave similarly. Therefore, the results of this study also apply to the original algorithm.

Since HYPR is a noniterative algorithm, it is expected to be more applicable in clinical practice than iterative approaches, such as the assignment and update with correlation (AUCTION) algorithm (7). On the other hand, the iterative approaches are expected to be more flexible in terms of controlling artifacts. As shown in Fig. 9, with the model used in Fig. 3, AUCTION reconstruction has significantly less signal modulation than the eight-projection HYPR reconstruction. However, AUCTION reconstruction is currently limited to using two orthogonal projections. There are technical challenges to add more projections into the algorithm. Therefore, the current AUCTION algorithm has stricter requirements in terms of data sparsity to avoid ambiguities in the reconstruction. There is potential to apply the HYPR images as more precise temporal constraints to the AUCTION reconstruction, thereby reducing the potential ambiguities of the iterative reconstruction.

One assumption of HYPR reconstruction is that no motion exists during data acquisition. Motion will blur the composite image and induce artifacts in normalization. However, motion can potentially be corrected by knowing the relative position of the object from the limited projections, in a similar manner as in Periodically Rotated Overlapping Parallel Lines with Enhanced Reconstruction (PROPELLER) (13). This should be investigated in future studies.

CONCLUSION

The reliability of HYPR reconstruction depends on the data sparsity and the uniformity of temporal dynamics. In contrast-enhanced MRA, data sparsity and signal uniformity are in general satisfied to produce HYPR-reconstructed images with limited artifacts. When contrast dy-

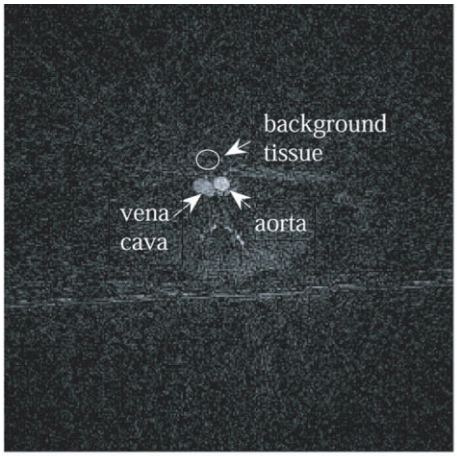

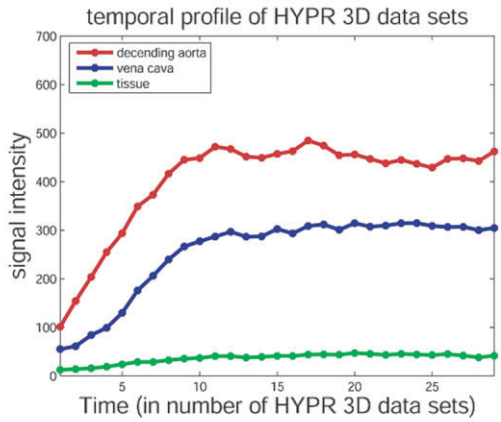

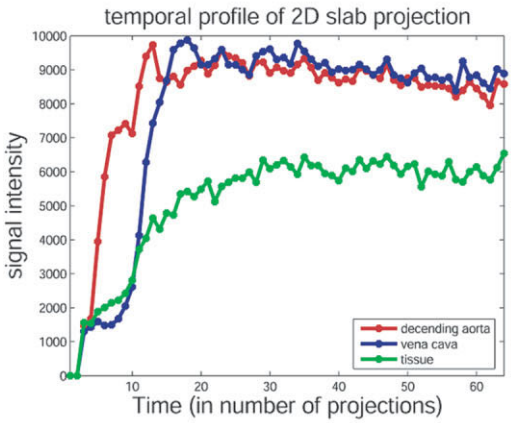

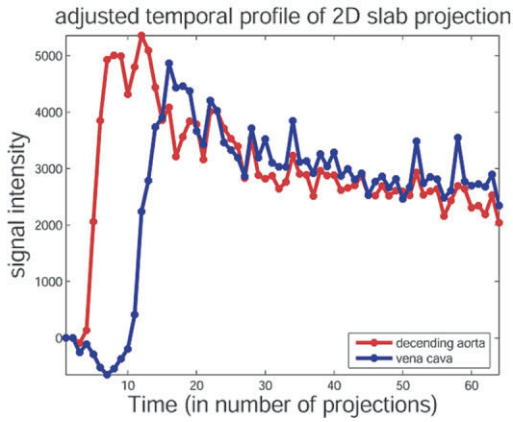

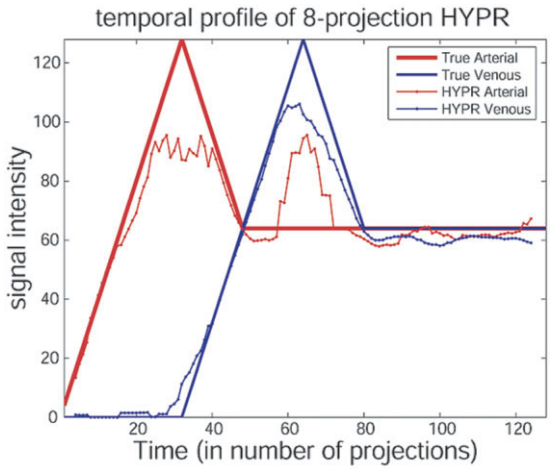

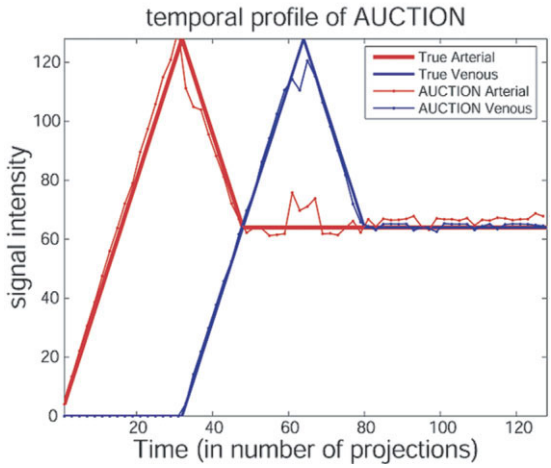

FIG. 9. Comparison of the temporal profiles of 8-projection HYPR reconstruction and the AUCTION reconstruction of the model used in Fig. 3. AUCTION reconstruction has less signal modulation for this model at the expense of significantly longer reconstruction time due to its iterative approach.

namics vary over space, large vessels (e.g., veins) tend to introduce more signal interference to small vessels (e.g., arteries) in HYPR, particularly when the vessels are in close proximity. The modulation of the steady-state arterial and venous signals by enhanced background tissue signals should also be taken into consideration. However, the artifacts are manifest as intensity modulation rather than structural interference, and therefore have little im-

FIG. 8. Measurement of the effect of background enhancement on HYPR with in-vivo data. **a:** Illustrates the regions-of-interest (ROIs) of the arterial signals (descending aorta), venous signals (vena cava) and background tissues in a cross-sectional HYPR image of the in vivo study shown in Fig. 7. The temporal profiles of the ROIs in the HYPR reconstruction are shown in (**b**). In (**c**), the increase of the background tissue signals is significant in the single-view projection images, which also increases intensities of arterial and venous ROIs. In (**d**), the arterial and venous signals are adjusted by subtracting the tissue signals, and therefore drop to a similar steady-state level as expected.

pact on structural diagnosis. Increasing the number of projections per time point increases temporal blur while reducing corruption of temporal behavior from adjacent objects. A uniform acquisition order, such as the bit-reversed order, is required to reduce imaging artifacts. An attractive feature of HYPR is that SNR is not sacrificed by improved temporal resolution. Therefore, HYPR reconstruction has potential to greatly improve time-resolved MRA in clinical practice, although results should be interpreted in light of expected artifacts described here.

ACKNOWLEDGEMENTS

We thank Charles Mistretta for helpful discussions on the modified algorithm. We also thank Michael Bronskill and Rajiv Chopra for cooperating on the animal studies.

REFERENCES

1. Wilman AH, Riederer SJ, King BF, Debbins JP, Rossman PJ, Ehman RL. Fluoroscopically triggered contrast-enhanced three-dimensional MR angiography with elliptical centric view order: application to the renal arteries. Radiology 1997;205:137–146.
2. Watts R, Wang Y, Redd B, Winchester PA, Kent KC, Bush HL, Prince MR. Recessed elliptical-centric view-ordering for contrast enhanced 3D MR angiography of the carotid arteries. Magn Reson Med 2002;48:419–424.
3. Maki JH, Wilson GJ, Eubank WB, Hoogeveen RM. Utilizing SENSE to achieve lower station sub-millimeter isotropic resolution and minimal venous enhancement in peripheral MR angiography. J Magn Reson Imaging 2002;15:484–491.
4. Prince MR, Chabra SG, Watts R, Chen CZ, Winchester PA, Khilnani NM, Trost D, Bush HA, Kent KC, Wang Y. Contrast material travel times in patients undergoing peripheral MR angiography. Radiology 2002; 224:55–61.
5. Peters DC, Korosec FR, Grist TM, Block WF, Holden JE, Vigen KK, Mistretta CA. Undersampled projection reconstruction applied to MR angiography. Magn Reson Med 2000;43:91–101.
6. Barger AV, Block WF, Toropov Y, Grist TM, Mistretta CA. Time-resolved contrast-enhanced imaging with isotropic resolution and broad coverage using an undersampled 3D projection trajectory. Magn Reson Med 2002;48:297–305.
7. Huang Y, Gurr D, Wright GA. Three-dimensional reconstruction of limited-view projections for contrast-enhanced magnetic resonance angiography at high temporal and spatial resolution. Magn Reson Med 2006;55:68–74.
8. Mistretta CA, Wieben O, Velikina J, Block W, Perry J, Wu Y, Johnson K, Wu Y. Highly constrained backprojection for time-resolved MRI. Magn Reson Med 2006;55:30–40.
9. Korosec FR, Frayne R, Grist TM, Mistretta CA. Time-resolved contrast-enhanced 3D MR angiography. Magn Reson Med 1996;36:345–351.
10. Spielman DM, Pauly JM, Meyer CH. Magnetic resonance fluoroscopy using spirals with variable sampling densities. Magn Reson Med 1995; 34:388–394.
11. Tsao J, Boesiger P, Pruessmann KP. Lattice permutation for reducing motion artifacts in radial and spiral dynamic imaging. Magn Reson Med 2006;55:116–125.
12. Winkelmann S, Schaeffter T, Eggers H, Nielsen T, Doessel O. Single shot T1-mapping, using a radial look-locker sequence and an optimal profile order determined by the golden cut rule. In: Proceedings of the 13th Annual Meeting of ISMRM, Miami Beach, FL, USA, 2005 (Abstract 2196).
13. Pipe JG. Motion correction with PROPELLER MRI: application to head motion and free-breathing cardiac imaging. Magn Reson Med 1999;42: 963–969.